

APPENDIX 1

Retrieval of water-leaving radiance and aerosol optical thickness over the oceans with SeaWiFS: A preliminary algorithm

by

Howard R. Gordon and Menghua Wang

Department of Physics
University of Miami
Coral Gables, FL 33124

(Accepted for Publication in *Applied Optics*)

Acknowledgement

This work received support from the National Aeronautics and Space Administration under Grant NAGW-273 and Contracts NAS5-31363 and NAS5-31743.

Abstract

The second generation of ocean color instruments require more accurate atmospheric correction than the Coastal Zone Color Scanner (CZCS) in order to utilize fully their increased radiometric sensitivity. Unlike CZCS, they will possess bands in the near infrared (NIR) placed solely for aiding atmospheric correction. It is shown, using aerosol models, that certain assumptions regarding the spectral behavior of the aerosol reflectance employed in the standard CZCS correction algorithm are not valid over the spectral range encompassing both the visible and NIR. Furthermore, it is shown that multiple scattering effects on the algorithm depend significantly on the aerosol model. Following these observations, an algorithm is proposed to utilize the NIR bands for atmospheric correction to the required accuracy. Examples of the dependence of the error on the aerosol model, the turbidity of the atmosphere, and the presence of surface roughness (waves) are provided. The error in the retrieved phytoplankton pigment concentration (the principal product of ocean color sensors) induced by errors in the atmospheric correction are shown to be $< 20\%$ in approximately 90% of the cases examined. Finally, the aerosol optical thickness (τ_a) is estimated through a simple extension of the correction algorithm. Simulations suggest that the error in the recovered value of τ_a should be $\lesssim 10\%$.

Introduction

The Coastal Zone Color Scanner (CZCS) on Nimbus-7 was a scanning radiometer which viewed the ocean in six co-registered spectral bands, five in the visible and near infrared (443, 520, 550, 670, and 750 nm, labeled bands 1, 2, 3, 4, and 5, respectively) and one in the thermal infrared (10.5 – 12.5 μm , band 6). The purpose of the CZCS was to provide estimates of the near-surface concentration of phytoplankton pigments by measuring the radiance backscattered out of the water.¹⁻³ Only the first four bands (henceforth referred to as λ_1 , λ_2 , λ_3 , and λ_4) had sufficient radiometric sensitivity to be useful for this. The next generation ocean color sensors, such as the Sea-viewing-Wide-Field-of-view-Sensor (SeaWiFS)⁴ and the Moderate Resolution Imaging Spectroradiometer (MODIS),⁵ will have a radiometric sensitivity superior to CZCS (through an increased signal to noise ratio and a smaller quantization interval). They also will be equipped with additional spectral bands, e.g., a band near 412 nm to separate the detrital and viable phytoplankton signals, and bands centered on 765 and 865 nm to aid atmospheric correction. Our goal is to refine the CZCS

atmospheric correction algorithm⁶⁻¹² to utilize the new spectral bands and the increased sensitivity in order to improve the accuracy of the pigment retrieval. A by-product of this atmospheric correction algorithm is an estimate of the aerosol optical thickness.

In earlier papers^{13,14} we simulated the influence of wind-induced sea surface roughness on the quality of the retrieval of the water-leaving radiances from an ocean color sensor when a CZCS-type algorithm, which assumes a *flat* ocean, is used. We reached three significant conclusions for situations in which there is no direct sun glitter in the image (either a large solar zenith angle or the sensor tilted away from the specular image of the sun). First, the error induced by ignoring the surface roughness is usually $\lesssim 1$ CZCS digital count for wind speeds up to ≈ 17 m/s, and therefore can be ignored for that sensor. Next, the roughness-induced error is much more strongly dependent on the wind speed than on the shadowing of one wave by another, suggesting that surface effects can be adequately dealt with without a precise knowledge of wave shadowing. Finally, the error induced by ignoring the multiple scattering is usually larger than that caused by ignoring the surface roughness, suggesting that, in refining algorithms for future sensors, more effort should be placed on dealing with multiple scattering than on the roughness of the sea surface. In the present paper, we present a preliminary algorithm for the atmospheric correction of the more-sensitive SeaWiFS instrument.

We begin by reviewing the CZCS correction algorithm and show that CZCS does not have a sufficient number of spectral bands to permit atmospheric correction on a pixel-by-pixel basis without the introduction of additional assumptions. Next, we examine the possibility of employing the additional spectral bands in the NIR to effect an atmospheric correction under the assumption of single scattering. Finally, we propose a scheme for dealing with multiple scattering which leads to the preliminary algorithm.

CZCS Correction Algorithm

We begin with the definition of reflectance ρ :

$$\rho = \pi L / F_0 \cos \theta_0, \quad (1)$$

where L is the upward radiance in the given viewing direction, F_0 is the extraterrestrial solar irradiance, and θ_0 is the solar zenith angle. With this normalization for L , ρ determined at the top of the atmosphere would be the albedo of the ocean-atmosphere system if L were independent of the viewing angle. Because it is often more convenient to work with dimensionless reflectance (ρ) rather than radiance (L), and because the new sensors may be calibrated in reflectance instead of radiance, we shall abandon L in favor of ρ in this paper. Note, however, that given F_0 , the transformation from one to the other is trivial. We can write the total reflectance, at a wavelength λ , measured at the top of the atmosphere as

$$\rho_t(\lambda) = \rho_r(\lambda) + \rho_a(\lambda) + \rho_{ra}(\lambda) + \rho_g(\lambda) + t\rho_w(\lambda), \quad (2)$$

where ρ_r is the reflectance resulting from multiple scattering by air molecules (Rayleigh scattering) in the absence of aerosols, ρ_a is the reflectance resulting from multiple scattering by aerosols in the absence of the air, ρ_{ra} is the interaction term between molecular and aerosol scattering,¹⁵ ρ_g is the reflectance of the direct solar beam, i.e., photons that are specular reflected from the (rough) ocean surface, and ρ_w is the water-leaving reflectance. The ρ_g term in the above equation is generally ignored because ocean color sensors are equipped with a provision for tilting the scan plane away from the specular image of the sun. It will also be ignored here. The term ρ_{ra} accounts for the interaction between Rayleigh and aerosol scattering, e.g., photons first scattered by the air then scattered by aerosols, or photons first scattered by aerosols then air, etc. This term is zero in the single scattering case, in which photons are only scattered once, and can be ignored as long as the amount of multiple scattering is small, i.e., at small Rayleigh and aerosol optical thicknesses.

The purpose of atmospheric correction is to retrieve ρ_w from the above equation. In principle the reflectances $\rho_r + \rho_a + \rho_{ra}$ could be removed if the concentration and optical properties of the aerosol were known throughout an image. The aerosol, however, is highly variable, and, unlike the Rayleigh scattering component ρ_r , the effects of $\rho_a + \rho_{ra}$ on the imagery cannot be predicted a priori. In the CZCS atmospheric correction algorithm the term ρ_{ra} is ignored, and it is assumed that ρ_a can be replaced by its *single scattering* value ρ_{as} .^{7,8,10-12,16} Equation (2) then becomes

$$\rho_t(\lambda) = \rho_r(\lambda) + \rho_{as}(\lambda) + t\rho_w(\lambda), \quad (3)$$

where

$$\rho_{as}(\lambda) = \omega_a(\lambda)\tau_a(\lambda)p_a(\theta, \theta_0, \lambda)/4 \cos\theta \cos\theta_0, \quad (4)$$

$$p_a(\theta, \theta_0, \lambda) = P_a(\theta_-, \lambda) + \left(r(\theta) + r(\theta_0) \right) P_a(\theta_+, \lambda),$$

$$\cos \theta_{\pm} = \pm \cos \theta_0 \cos \theta - \sin \theta_0 \sin \theta \cos(\phi - \phi_0),$$

and $r(\theta)$ is the Fresnel reflectance of the interface for an incident angle θ . The parameters $\tau_a(\lambda)$, $\omega_a(\lambda)$, and $P_a(\alpha, \lambda)$ are, respectively, the aerosol optical thickness, the aerosol single scattering albedo, and the aerosol scattering phase function for a scattering angle α . The angles θ_0 and ϕ_0 are, respectively, the zenith and azimuth angles of a vector from the point on the sea surface under examination (pixel) to the sun, and likewise, θ and ϕ are the zenith and azimuth angles of a vector from the pixel to the sensor. In what follows we take $\phi_0 = 0$.

The general approach of the correction algorithm is to use spectral bands for which ρ_w is known, to make an assessment of the aerosol contribution. For this, one band is required to assess the magnitude of the aerosol's contribution, and a second is required to assess its dependence on wavelength. Also, to extrapolate (or interpolate) the aerosol contribution to the other bands, a rule governing the spectral variation of ρ_{as} is required. For clear ocean water (phytoplankton pigment concentration, C , less than 0.25 mg/m^3) ρ_w can be considered known¹⁶ for bands 2, 3, and 4. Thus, in clear water there are enough spectral bands to estimate $\rho_w(\lambda_1)$, which is a very sensitive function of C , and can be used to estimate the actual value of C . In the past, the error in the retrieved $\rho_w(\lambda_1)$ in clear water has been used in numerical simulations to study the efficacy of the correction algorithm and its assumptions.^{11,14} It will be used in the same manner here.

The algorithm is operated by defining the atmospheric correction parameters $\varepsilon(\lambda_i, \lambda_j)$:

$$\varepsilon(\lambda_i, \lambda_j) \equiv \frac{\rho_{as}(\lambda_i)}{\rho_{as}(\lambda_j)} = \frac{\omega_a(\lambda_i)\tau_a(\lambda_i)p_a(\theta, \theta_0, \lambda_i)}{\omega_a(\lambda_j)\tau_a(\lambda_j)p_a(\theta, \theta_0, \lambda_j)}. \quad (5)$$

Then, we compute $\varepsilon(\lambda_2, \lambda_4)$, $\varepsilon(\lambda_3, \lambda_4)$, and $\varepsilon(\lambda_4, \lambda_4)$ from $\rho_{as}(\lambda_2)$, $\rho_{as}(\lambda_3)$, and $\rho_{as}(\lambda_4)$, and extrapolate to find $\varepsilon(\lambda, \lambda_4)$ for any λ , e.g., λ_1 , by assuming that

$$\varepsilon(\lambda, \lambda_4) = \left(\frac{\lambda_4}{\lambda} \right)^n. \quad (6)$$

Finally, $\rho_{as}(\lambda_1) = \varepsilon(\lambda_1, \lambda_4)\rho_{as}(\lambda_4)$, yielding $t(\lambda_1)\rho_w(\lambda_1)$ via Eq. (3). t is the diffuse transmittance of the atmosphere given approximately by⁹

$$t = \exp[-(\tau_r/2 + \tau_{O_2})/\cos \theta],$$

where τ_r is the ‘‘Rayleigh’’ optical thickness (molecular scattering) and τ_{O_3} is the Ozone optical thickness. Note the requirement of *at least* two bands for which ρ_w is given (three are available in this example) so that ρ_{as} can be computed, and the need for an extrapolation ‘‘law,’’ i.e., Eq. (6).

For pigment concentrations greater than 0.25 mg/m^3 , ρ_w is no longer known for bands 2 and 3 so this procedure cannot be applied. One procedure that has been used is to first locate clear water in the image, then apply the above procedure, and finally use the resulting ε -values for the entire image.⁹ The drawbacks to this are the paucity of clear water in many images and the fact that the true ε may not be constant over the image. Morel and co-workers^{17,18} have devised an alternate approach that uses a model-produced relationship between $\rho_w(\lambda_i)$ and C , *assumes* Eq. (6) is valid with an unknown n , and solves the resulting nonlinear equations at each pixel for C and n by iteration. However, the fact remains that, except in clear water, there is not sufficient information to perform atmospheric correction in the *general* case. In fact, thus far in the analysis of the CZCS global data set,¹⁹ the values of ε have been set to unity (a very plausible value for marine aerosols) for all of the processing in order to effect a solution.

Application of the CZCS Algorithm to SeaWiFS

The next ocean color sensor to fly in space is the Sea-viewing-Wide-Field-of-view-Sensor⁴ (SeaWiFS). The radiometric specifications for SeaWiFS are presented in Table 1, in which ρ_{max} is the saturation reflectance, ρ_w is the water-leaving reflectance for clear ocean water, e.g., the Sargasso Sea, ρ_t is a typical value of the total radiance and $NE\Delta\rho$ is the noise equivalent reflectance.

Table 1: SeaWiFS Performance for $\theta_0 = 60^\circ$ at the Scan Edge

Band	λ (nm)	ρ_{max}	ρ_w	ρ_t	$NE\Delta\rho$
1	402–422	0.50	0.040	0.34	0.00068
2	433–453	0.46	0.038	0.29	0.00043
3	480–500	0.36	0.024	0.23	0.00034
4	500–520	0.30	0.0096	0.19	0.00031
5	545–565	0.25	0.0040	0.154	0.00027
6	660–680	0.17	0.0004	0.105	0.00023
7	745–785	0.15	–	0.081	0.00018
8	845–885	0.13	–	0.069	0.00015

Since ρ_w is essentially zero for SeaWiFS bands 7 and 8, it is logical to use these bands to assess the aerosol properties, i.e., to determine $\varepsilon(765, 865) = \rho_{as}(765)/\rho_{as}(865)$ and use it to deduce $\varepsilon(\lambda, 865)$. However, noting that the total spectral region covered varies by over a factor of two in wavelength, it is not clear that the extrapolation provided by Eq. (6) will be valid.

In order to try to gain some insight into the possible behavior of $\varepsilon(\lambda, 865)$, we have computed it for several aerosol models. The aerosol models we used were developed by Shettle and Fenn²⁰ for LOWTRAN-6.²¹ In particular, we considered their Maritime and Tropospheric models, and introduced a Coastal model containing half the fraction of the sea salt aerosol that was in the Maritime model. The Coastal model simulates situations that may be expected to occur near the coast (larger continental influence). From the resulting size distributions and refractive indices, we used Mie theory to compute the aerosol optical properties for the SeaWiFS bands as a function of the relative humidity (RH). From these, $\varepsilon(\lambda, 865)$ is found. Sample results of this exercise are presented in Figures 1a and 1b. These computations suggest that there should be a strong variation of ε with aerosol model and RH. The increase in particle size (due to swelling) with increasing RH clearly reduces the spectral variation of ε . The spectral variation of ε is due in large part to the spectral variation of τ_a ; however, additional variation is produced by the aerosol phase function, which was assumed to be independent of λ in the earlier CZCS algorithm.

Equation (6) suggests that there is a linear relationship between $\log(\varepsilon)$ and $\log(\lambda)$ of slope $-n$; however, Figure 1b, which provides the computations in Figure 1a plotted in this format, shows that for most models this is a poor approximation for the variation of $\varepsilon(\lambda, 865)$ taken over the entire range of λ . Nevertheless, it is interesting to note that over the restricted range 443 to 670 nm, Eq. (6) is a reasonable approximation, and that using it to extrapolate ε from 520, 550, and 670 nm to 443 nm can be quite accurate. This may explain the success of such extrapolations with CZCS.

Continuing with the single scattering approximation, we can estimate the error $\Delta\varepsilon$ that can be tolerated in ε for a given error in $t(\lambda)\Delta\rho_w(\lambda)$. This is

$$\Delta\varepsilon(\lambda, 865)\rho_{as}(865) = -t(\lambda)\Delta\rho_w(\lambda).$$

A goal of SeaWiFS is to be able to recover ρ_w with an error of no more than 5%. For clear water ($C \lesssim 0.2 \text{ mg/m}^3$) at 443 nm, $\rho_w \gtrsim 0.02$ which implies the error in $\rho(443)$, $\Delta\rho_w(443)$, should be

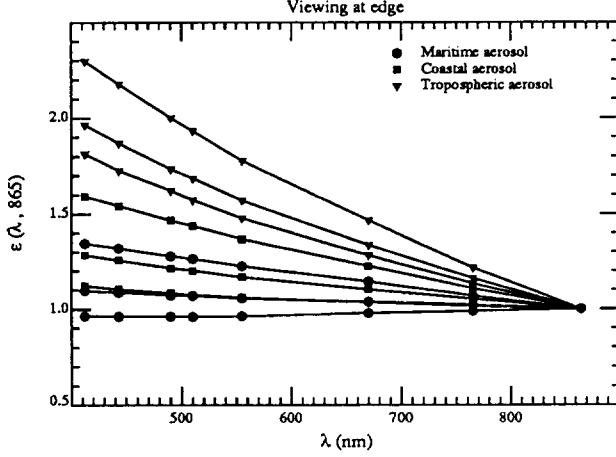


Figure 1a. $\varepsilon(\lambda, 865)$ as a function of λ at the edge of the SeaWiFS scan ($\theta \approx 45^\circ$, $\phi = 90^\circ$) with $\theta_0 = 60^\circ$ for the Maritime, Coastal, and Tropospheric aerosol models. For each model, the RH values are 70%, 90%, and 98% from the upper to the lower curves.

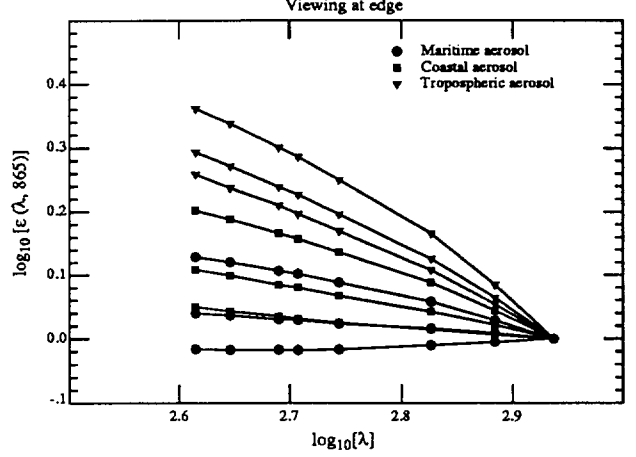


Figure 1b. $\varepsilon(\lambda, 865)$ as a function of λ at the edge of the SeaWiFS scan ($\theta \approx 45^\circ$, $\phi = 90^\circ$) with $\theta_0 = 60^\circ$ for the Maritime, Coastal, and Tropospheric aerosol models. For each model, the RH values are 70%, 90%, and 98% from the upper to the lower curves.

$\lesssim 0.001$. Ignoring the factor t , which is between 0.8 and 0.9, we have

$$\Delta\varepsilon(443, 865) \approx \pm \frac{0.001}{\rho_{as}(865)}.$$

Since $\rho_{as} \propto \tau_a$, the required accuracy in $\varepsilon(443, 865)$ is increased as the turbidity of the atmosphere increases. Reddy et al.²² report a mean τ_a over the North Atlantic of ≈ 0.1 near 800 nm in situations where air mass trajectory analysis suggests the presence of only a maritime aerosol, and ≈ 0.2 when both continental and marine aerosols are expected to be present. Using the Maritime or Coastal models with RH = 90% to represent these two situations, the model predicts (for $\theta_0 = 60^\circ$ at the scan edge) that $\rho_{as}(865) \approx 0.066 \tau_a(865)$. Thus,

$$\Delta\varepsilon(443, 865) \lesssim \pm \frac{0.015}{\tau_a(865)}$$

should lead to an error of less than 5% in $\rho_w(443)$ in clear water. This yields $\Delta\varepsilon \lesssim 0.15$ and 0.08 for $\tau_a = 0.1$ and 0.2, respectively. Thus, under average conditions in the North Atlantic, we must require $\Delta\varepsilon \lesssim \pm 0.10$ (or $\Delta \log \varepsilon \lesssim \pm 0.043/10^{\log \varepsilon}$ for Figure 1b) for $\theta_0 = 60^\circ$ at the scan edge. Figure 1b shows that this limit is not met when ε is extrapolated according to Eq. (6) and RH < 90% for the Maritime and Coastal models, or for any of the Tropospheric models. Figure 1a shows that a linear extrapolation ($\varepsilon \propto \lambda$) does not perform significantly better in this example.

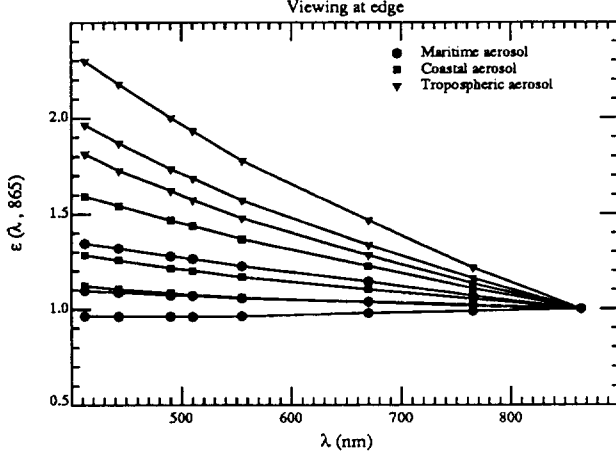


Figure 1a. $\varepsilon(\lambda, 865)$ as a function of λ at the edge of the SeaWiFS scan ($\theta \approx 45^\circ$, $\phi = 90^\circ$) with $\theta_0 = 60^\circ$ for the Maritime, Coastal, and Tropospheric aerosol models. For each model, the RH values are 70%, 90%, and 98% from the upper to the lower curves.

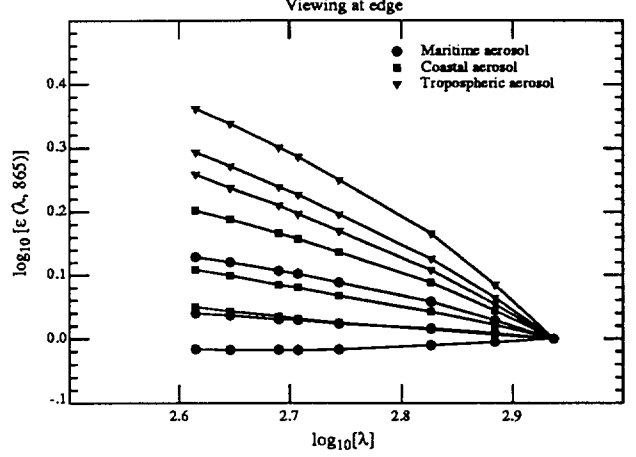


Figure 1b. $\varepsilon(\lambda, 865)$ as a function of λ at the edge of the SeaWiFS scan ($\theta \approx 45^\circ$, $\phi = 90^\circ$) with $\theta_0 = 60^\circ$ for the Maritime, Coastal, and Tropospheric aerosol models. For each model, the RH values are 70%, 90%, and 98% from the upper to the lower curves.

$\lesssim 0.001$. Ignoring the factor t , which is between 0.8 and 0.9, we have

$$\Delta\varepsilon(443, 865) \approx \pm \frac{0.001}{\rho_{as}(865)}.$$

Since $\rho_{as} \propto \tau_a$, the required accuracy in $\varepsilon(443, 865)$ is increased as the turbidity of the atmosphere increases. Reddy et al.²² report a mean τ_a over the North Atlantic of ≈ 0.1 near 800 nm in situations where air mass trajectory analysis suggests the presence of only a maritime aerosol, and ≈ 0.2 when both continental and marine aerosols are expected to be present. Using the Maritime or Coastal models with RH = 90% to represent these two situations, the model predicts (for $\theta_0 = 60^\circ$ at the scan edge) that $\rho_{as}(865) \approx 0.066 \tau_a(865)$. Thus,

$$\Delta\varepsilon(443, 865) \lesssim \pm \frac{0.015}{\tau_a(865)}$$

should lead to an error of less than 5% in $\rho_w(443)$ in clear water. This yields $\Delta\varepsilon \lesssim 0.15$ and 0.08 for $\tau_a = 0.1$ and 0.2, respectively. Thus, under average conditions in the North Atlantic, we must require $\Delta\varepsilon \lesssim \pm 0.10$ (or $\Delta \log \varepsilon \lesssim \pm 0.043/10^{\log \varepsilon}$ for Figure 1b) for $\theta_0 = 60^\circ$ at the scan edge. Figure 1b shows that this limit is not met when ε is extrapolated according to Eq. (6) and RH < 90% for the Maritime and Coastal models, or for any of the Tropospheric models. Figure 1a shows that a linear extrapolation ($\varepsilon \propto \lambda$) does not perform significantly better in this example.

Under extreme conditions, $\tau_a(865)$ can be significantly larger than 0.2 and still not saturate the sensor (see Table 5 below). In these cases the required $\Delta\varepsilon$ will be correspondingly smaller. We conclude then that to the extent that these aerosol models approximate reality, they suggest that a simple extrapolation of the derived value of $\varepsilon(765, 865)$, or even $\varepsilon(670, 765)$ or $\varepsilon(670, 865)$, to shorter wavelengths will be *difficult*, and limits the accuracy of the algorithm in this simplified (single scattering) analysis.

A possible scheme for improving extrapolation is to base it on models [or on an experimental data base of $\varepsilon(765, 865)$ values], e.g., if the derived value of $\varepsilon(765, 865)$ falls midway between the values predicted by two models, we assume that $\varepsilon(\lambda, 865)$ will also fall midway between the two models for all λ , etc. We have applied this idea to try to derive $\varepsilon(443, 865)$ from $\varepsilon(765, 865)$ for the Maritime, Coastal, and Tropospheric aerosols at RH = 80%. For the cases examined below, i.e., $\theta_0 = 0^\circ, 20^\circ, 40^\circ$, and 60° , at both the scan center and scan edge, $\Delta\varepsilon(443, 865) < 0.02$ for all cases except one (where it was 0.0201), and was often < 0.01 . Thus, this assumption, that aerosols with similar $\varepsilon(765, 865)$ also have similar $\varepsilon(\lambda, 865)$, seems to be borne out by the aerosol models considered here; however, in the final analysis its validity must rest on experimental observations not now available. Given a well calibrated SeaWiFS, it will be possible to test the hypothesis by studying $\varepsilon(\lambda, 865)$ for $\lambda \gtrsim 520$ nm over clear water areas, for which $\rho_w(\lambda)$ is known.

Actually, we found that the variation of $\varepsilon(\lambda_i, \lambda_j)$ with wavelength, over the entire range of SeaWiFS bands, could be represented well by a simple formula of the form $\varepsilon(\lambda_i, \lambda_j) = \exp[c(\lambda_j - \lambda_i)]$, where c depends on the viewing geometry and the aerosol model. Extrapolation of $\varepsilon(765, 865)$ obtained using this formula was as good as that obtained using the models. In fact, we have used this observation to modify the CZCS algorithm for use with SeaWiFS.²³ The modified CZCS algorithm works reasonably well when $\tau_a(865)$ is small, e.g., when $\tau_a(865) = 0.2$, we find $\Delta\rho_w \lesssim \pm 0.002$ for the Maritime and the Coastal models compared with the required ± 0.001 . Unfortunately, it ignores multiple scattering, and the performance of the modified CZCS algorithm degrades rapidly as $\tau_a(865)$ increases, e.g, when $\tau_a(865) = 0.4$ with the Tropospheric model at RH = 80%, $\Delta\rho_w(440) \leq -0.04$ at the edge of the SeaWiFS scan with $\theta_0 = 60^\circ$ compared to -0.006 using an algorithm that includes multiple scattering as described below. Since the aerosol models seem to be required to address multiple scattering (next section), we chose to use them to effect the ε extrapolation as well.

Multiple Scattering

Our analysis thus far has been based on the assumption of single scattering; however, multiple scattering effects have been shown^{11,12,15} to be significant at the level of accuracy required for SeaWiFS, i.e., $\Delta\rho_w(443) \approx 0.001$. The single scattering solution has been used to simplify the mathematics, to demonstrate the ε -extrapolation difficulty, and to suggest an approach for the correction. It has also been used in the spirit that, if the correction cannot be made — at least conceptually — at the required accuracy in a singly scattering atmosphere, it is hopeless in a multiply scattering regime.

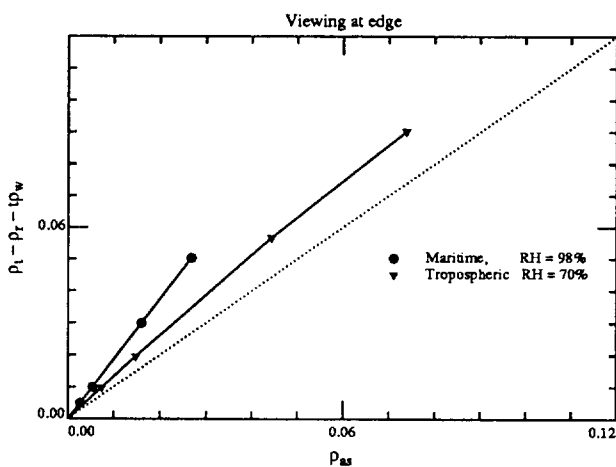


Figure 2a. $\rho_a(\lambda) + \rho_{ra}(\lambda)$ as a function of $\rho_{as}(\lambda)$ for $\lambda = 443$ nm and $\theta_0 = 60^\circ$ at the edge of the SeaWiFS. Lower solid line is for the Tropospheric model with RH = 70%, upper solid line is for the Maritime model with RH = 98%, and the dotted line is the single scattering result. Points correspond to $\tau_a = 0.05, 0.1, 0.3,$ and 0.5 .

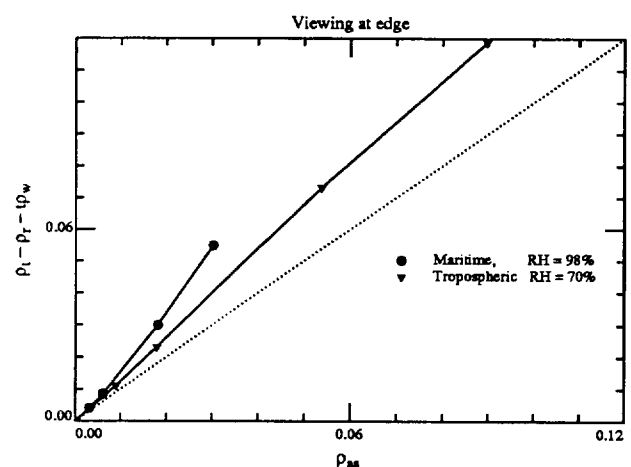


Figure 2b. $\rho_a(\lambda) + \rho_{ra}(\lambda)$ as a function of $\rho_{as}(\lambda)$ for $\lambda = 865$ nm and $\theta_0 = 60^\circ$ at the edge of the SeaWiFS. Lower solid line is for the Tropospheric model with RH = 70%, upper solid line is for the Maritime model with RH = 98%, and the dotted line is the single scattering result. Points correspond to $\tau_a = 0.05, 0.1, 0.3,$ and 0.5 .

When multiple scattering is included, atmospheric correction requires estimating the unknown $\rho_a(\lambda) + \rho_{ra}(\lambda)$ from its values at 765 and 865. These can be found since $\rho_w = 0$ at both wavelengths. Wang²⁴ has shown that a near-linear relationship exists between $\rho_a(\lambda) + \rho_{ra}(\lambda)$ and $\rho_{as}(\lambda)$. Examples of such a relationship are shown in Figures 2a and 2b at 443 and 865 nm, respectively, for the Tropospheric model with RH = 70% and the Maritime model with RH = 98%. At a given value of τ_a , the increase in reflectance from 443 to 865 nm in these figures is due to the fact that P_a is larger in backscattering directions at 865 than at 443 nm. The single scattering result (the 1:1 line), on which the preceding analysis was based, is also shown on the figures. The strong

Our analysis thus far has been based on the assumption of single scattering; however, multiple scattering effects have been shown^{11,12,15} to be significant at the level of accuracy required for SeaWiFS, i.e., $\Delta\rho_w(443) \approx 0.001$. The single scattering solution has been used to simplify the mathematics, to demonstrate the ϵ -extrapolation difficulty, and to suggest an approach for the correction. It has also been used in the spirit that, if the correction cannot be made — at least conceptually — at the required accuracy in a singly scattering atmosphere, it is hopeless in a multiply scattering regime.

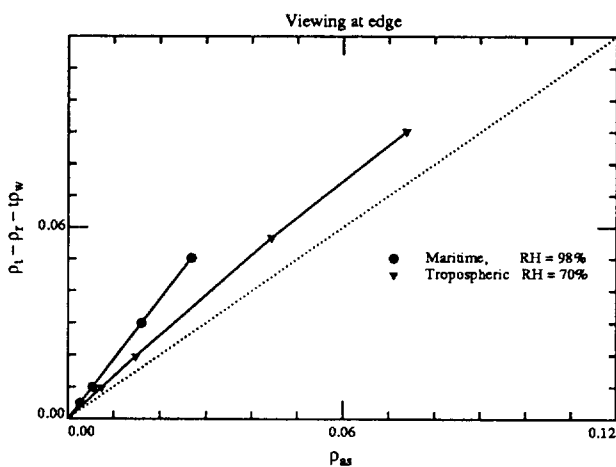


Figure 2a. $\rho_a(\lambda) + \rho_{ra}(\lambda)$ as a function of $\rho_{as}(\lambda)$ for $\lambda = 443$ nm and $\theta_0 = 60^\circ$ at the edge of the SeaWiFS. Lower solid line is for the Tropospheric model with RH = 70%, upper solid line is for the Maritime model with RH = 98%, and the dotted line is the single scattering result. Points correspond to $\tau_a = 0.05, 0.1, 0.3,$ and 0.5 .

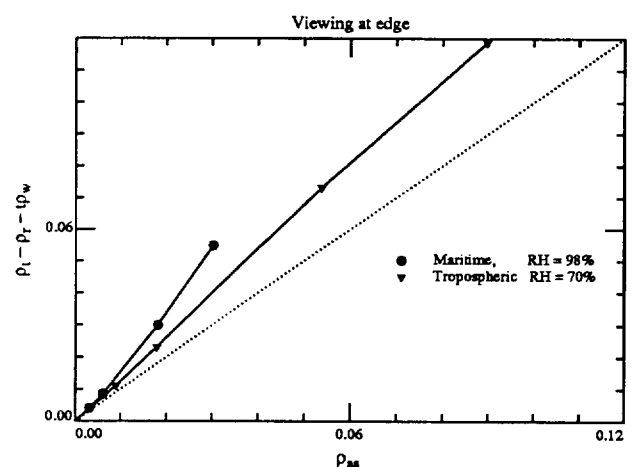


Figure 2b. $\rho_a(\lambda) + \rho_{ra}(\lambda)$ as a function of $\rho_{as}(\lambda)$ for $\lambda = 865$ nm and $\theta_0 = 60^\circ$ at the edge of the SeaWiFS. Lower solid line is for the Tropospheric model with RH = 70%, upper solid line is for the Maritime model with RH = 98%, and the dotted line is the single scattering result. Points correspond to $\tau_a = 0.05, 0.1, 0.3,$ and 0.5 .

When multiple scattering is included, atmospheric correction requires estimating the unknown $\rho_a(\lambda) + \rho_{ra}(\lambda)$ from its values at 765 and 865. These can be found since $\rho_w = 0$ at both wavelengths. Wang²⁴ has shown that a near-linear relationship exists between $\rho_a(\lambda) + \rho_{ra}(\lambda)$ and $\rho_{as}(\lambda)$. Examples of such a relationship are shown in Figures 2a and 2b at 443 and 865 nm, respectively, for the Tropospheric model with RH = 70% and the Maritime model with RH = 98%. At a given value of τ_a , the increase in reflectance from 443 to 865 nm in these figures is due to the fact that P_a is larger in backscattering directions at 865 than at 443 nm. The single scattering result (the 1:1 line), on which the preceding analysis was based, is also shown on the figures. The strong

multiple scattering, even at 865 nm, means that it must be removed in order to accurately estimate $\varepsilon(765, 865)$. We have experimented with several techniques for estimating $\varepsilon(765, 865)$. The best one we have found is to (1) assume that the aerosol belongs to a given aerosol model, e.g., the i^{th} model, (2) for the given geometry and model, solve the RTE and derive the $\rho_a(\lambda) + \rho_{ra}(\lambda)$ vs. $\rho_{as}(\lambda)$ relationships, (3) use these to estimate $\rho_{as}(765)$ and $\rho_{as}(865)$ to provide $\varepsilon_i(765, 865)$, and (4) average the ε 's derived for a large number (N) of likely models, i.e.,

$$\varepsilon(765, 865) = \frac{1}{N} \sum_{i=1}^N \varepsilon_i(765, 865).$$

This works reasonably well because the values of ε derived using the individual models are all close to the correct value, i.e., for any given model the multiple scattering effects are nearly the same at 765 and 865 nm. The weak Rayleigh scattering contribution at these wavelengths results in a very small ρ_{ra} .

Having derived a value for $\varepsilon(765, 865)$, the next task is to estimate $\varepsilon(\lambda, 865)$. In general, the derived value of $\varepsilon(765, 865)$ will fall between that for two of the N aerosol models. We then assume that $\varepsilon(\lambda, 865)$ falls between the same two aerosol models proportionately in the same manner as $\varepsilon(765, 865)$ as suggested above. Note that $\varepsilon(\lambda, 865)$ relates $\rho_{as}(\lambda)$ to $\rho_{as}(865)$; however, rather than $\rho_{as}(\lambda)$, we desire $\rho_a(\lambda) + \rho_{ra}(\lambda)$. Thus we must make a transformation similar to that in Figure 2a. We effect this by utilizing the two aerosol models that most closely bracketed $\varepsilon(765, 865)$, and assume that the $\rho_a(\lambda) + \rho_{ra}(\lambda)$ vs. $\rho_{as}(\lambda)$ relationship falls between that for the two aerosol models in the same proportion as $\varepsilon(765, 865)$.

The entire correction algorithm can be summarized schematically as follows,

$$\begin{aligned} t\rho_w(\lambda) &= \rho_t(\lambda) - \rho_r(\lambda) - [\rho_a(\lambda) + \rho_{ra}(\lambda)], \\ \underbrace{\rho_t - \rho_r}_{765, 865} &\xrightarrow{N \text{ Models}} \varepsilon(765, 865) \rightarrow 2 \text{ Models}, \\ \varepsilon(765, 865) &\xrightarrow{2 \text{ Models}} \varepsilon(\lambda, 865), \\ \rho_{as}(865) &\xrightarrow{\varepsilon(\lambda, 865)} \rho_{as}(\lambda), \\ \rho_{as}(\lambda) &\xrightarrow{2 \text{ Models}} \rho_a(\lambda) + \rho_{ra}(\lambda). \end{aligned}$$

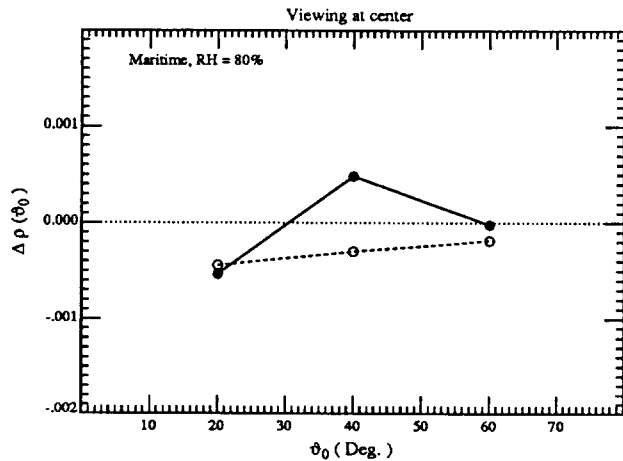


Figure 3a. Error in retrieved $t(443)\rho_w(443)$ for viewing at the center of the scan with a Maritime aerosol at RH = 80% as a function of the solar zenith angle. $\tau_a(865) = 0.2$.

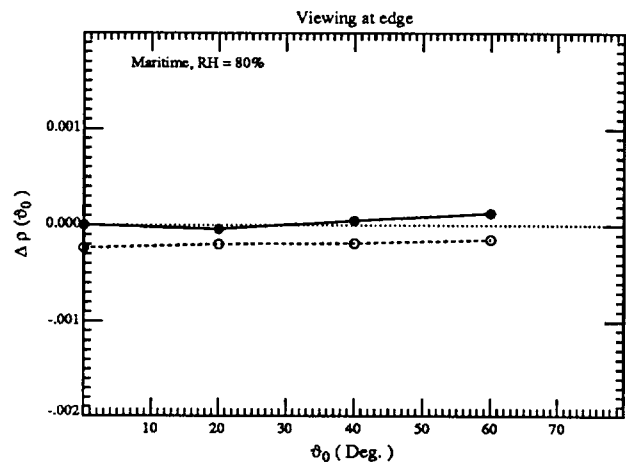


Figure 3b. Error in retrieved $t(443)\rho_w(443)$ for viewing at the edge of the scan with a Maritime aerosol at RH = 80% as a function of the solar zenith angle. $\tau_a(865) = 0.2$.

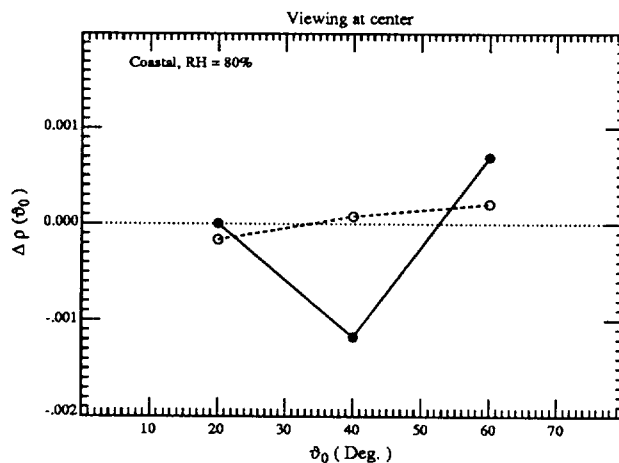


Figure 3c. Error in retrieved $t(443)\rho_w(443)$ for viewing at the center of the scan with a Coastal aerosol at RH = 80% as a function of the solar zenith angle. $\tau_a(865) = 0.2$.

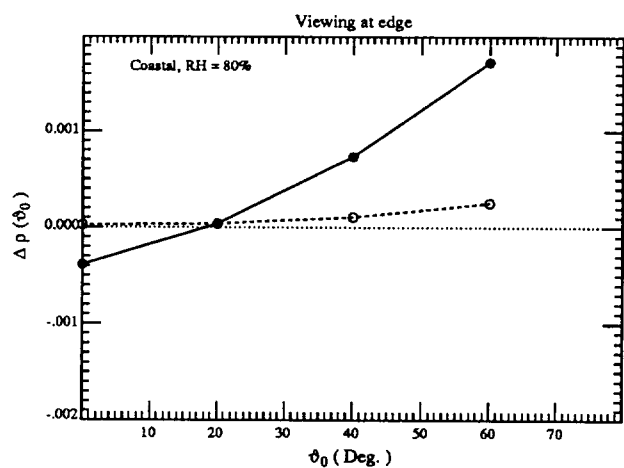


Figure 3d. Error in retrieved $t(443)\rho_w(443)$ for viewing at the edge of the scan with a Coastal aerosol at RH = 80% as a function of the solar zenith angle. $\tau_a(865) = 0.2$.

We note that the aerosol models used to address multiple scattering are those that most closely agree with the derived value of $\epsilon(765, 865)$. This places a premium on accurately deriving this quantity.

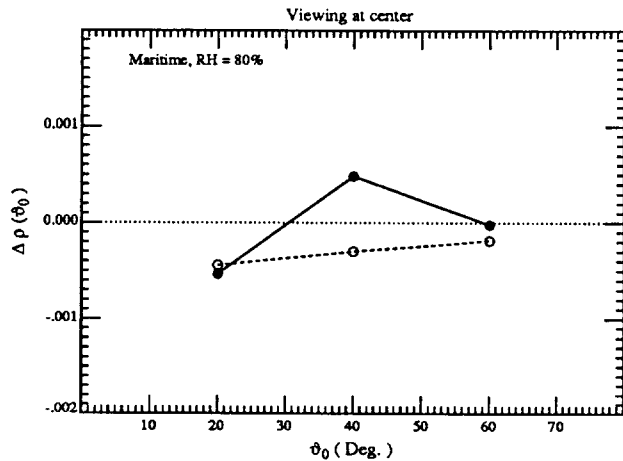


Figure 3a. Error in retrieved $t(443)\rho_w(443)$ for viewing at the center of the scan with a Maritime aerosol at RH = 80% as a function of the solar zenith angle. $\tau_a(865) = 0.2$.

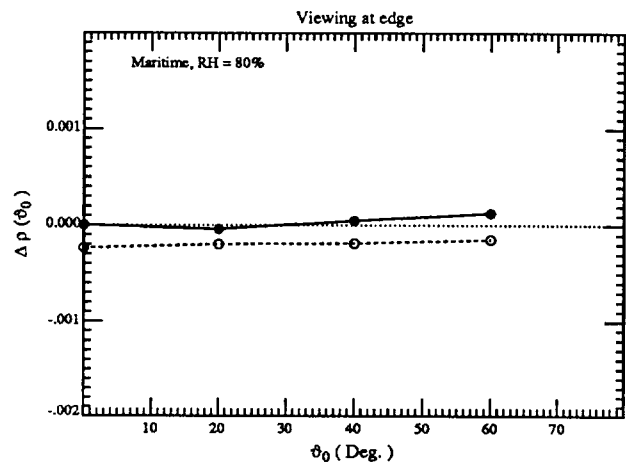


Figure 3b. Error in retrieved $t(443)\rho_w(443)$ for viewing at the edge of the scan with a Maritime aerosol at RH = 80% as a function of the solar zenith angle. $\tau_a(865) = 0.2$.

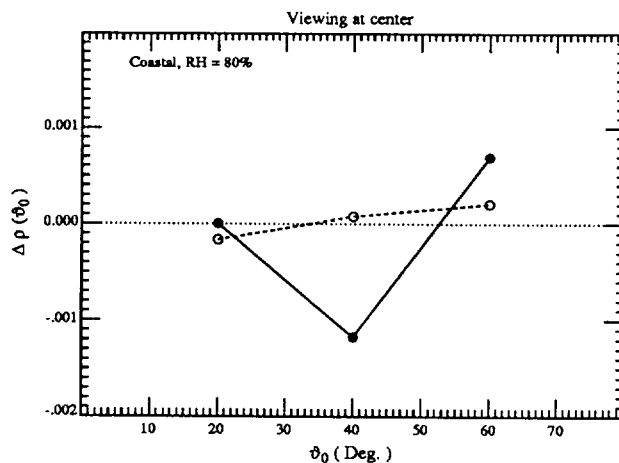


Figure 3c. Error in retrieved $t(443)\rho_w(443)$ for viewing at the center of the scan with a Coastal aerosol at RH = 80% as a function of the solar zenith angle. $\tau_a(865) = 0.2$.

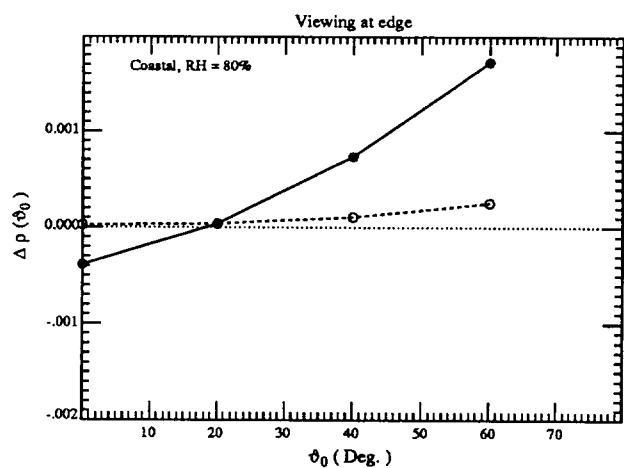


Figure 3d. Error in retrieved $t(443)\rho_w(443)$ for viewing at the edge of the scan with a Coastal aerosol at RH = 80% as a function of the solar zenith angle. $\tau_a(865) = 0.2$.

We note that the aerosol models used to address multiple scattering are those that most closely agree with the derived value of $\epsilon(765, 865)$. This places a premium on accurately deriving this quantity.

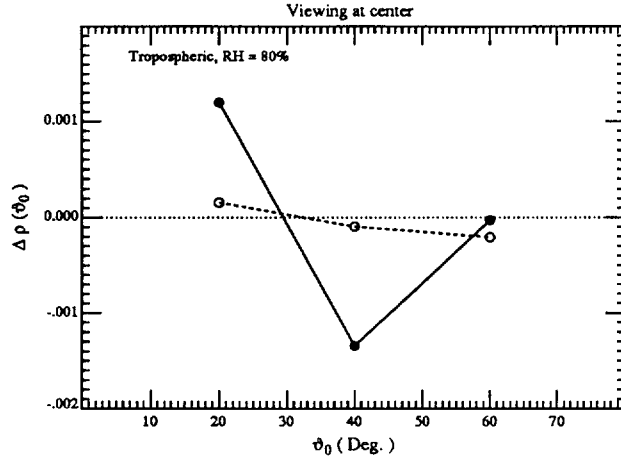


Figure 3e. Error in retrieved $t(443)\rho_w(443)$ for viewing at the center of the scan with a Tropospheric aerosol at $\text{RH} = 80\%$ as a function of the solar zenith angle. $\tau_a(865) = 0.2$.

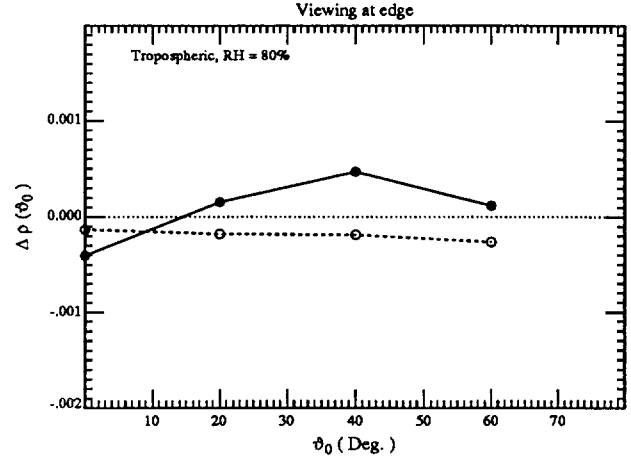


Figure 3f. Error in retrieved $t(443)\rho_w(443)$ for viewing at the edge of the scan with a Tropospheric aerosol at $\text{RH} = 80\%$ as a function of the solar zenith angle. $\tau_a(865) = 0.2$.

To try to assess the efficacy of these ideas, we have applied them to a series of simulations carried out using the models with $\text{RH} = 80\%$, i.e., $\rho_t(\lambda)$ was simulated [with $\rho_w(\lambda) = 0$] for $\text{RH} = 80\%$. These simulations were inserted into the above algorithm with the Maritime, Coastal, and Tropospheric models for $\text{RH} = 70, 90,$ and 98% serving as the $N = 9$ candidate aerosol models. The error in the recovered water-leaving reflectance, $\Delta\rho(\lambda) \equiv t(\lambda)\Delta\rho_w(\lambda)$, was computed. Note that the aerosol models used in the simulations were similar, but not identical, to any of the 9 candidate models. The simulations were carried out for $\theta_0 = 0, 20^\circ, 40^\circ,$ and 60° , the viewing was assumed to be at the center (nadir) and edge (viewing angle $\approx 45^\circ$, $\phi = 90^\circ$) of the scan. $\tau_a(865)$ was taken to be 0.2, which is about 2-3 times the average for the North Atlantic with a pure maritime atmosphere.²² The results are shown in Figures 3a to 3f (solid lines). There is no value plotted at the scan center for $\theta_0 = 0$ because in that viewing geometry ρ_t would be strongly contaminated by sun glitter. The results suggest that the proposed algorithm is close to producing the ± 0.001 accuracy in the water leaving reflectance at 443 nm under most circumstances.

Figures 3a–3f (dashed lines) also include the error in $t\rho_w$ that the algorithm would have if the correct physics of the atmosphere were single scattering, i.e., if the dotted lines on Figures 2a and 2b were applicable. In this case, $\epsilon(765, 865)$ is determined exactly, so the error is due entirely to the extrapolation from $\epsilon(765, 865)$ to $\epsilon(443, 865)$. Clearly, $t\Delta\rho_w$ is usually larger when there is

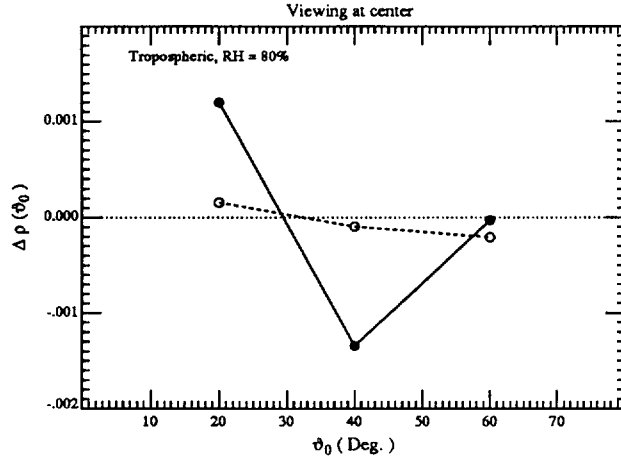


Figure 3e. Error in retrieved $t(443)\rho_w(443)$ for viewing at the center of the scan with a Tropospheric aerosol at $\text{RH} = 80\%$ as a function of the solar zenith angle. $\tau_a(865) = 0.2$.

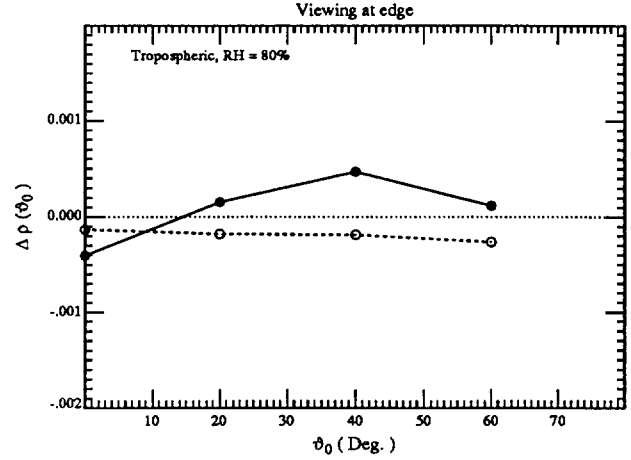


Figure 3f. Error in retrieved $t(443)\rho_w(443)$ for viewing at the edge of the scan with a Tropospheric aerosol at $\text{RH} = 80\%$ as a function of the solar zenith angle. $\tau_a(865) = 0.2$.

To try to assess the efficacy of these ideas, we have applied them to a series of simulations carried out using the models with $\text{RH} = 80\%$, i.e., $\rho_t(\lambda)$ was simulated [with $\rho_w(\lambda) = 0$] for $\text{RH} = 80\%$. These simulations were inserted into the above algorithm with the Maritime, Coastal, and Tropospheric models for $\text{RH} = 70, 90,$ and 98% serving as the $N = 9$ candidate aerosol models. The error in the recovered water-leaving reflectance, $\Delta\rho(\lambda) \equiv t(\lambda)\Delta\rho_w(\lambda)$, was computed. Note that the aerosol models used in the simulations were similar, but not identical, to any of the 9 candidate models. The simulations were carried out for $\theta_0 = 0, 20^\circ, 40^\circ,$ and 60° , the viewing was assumed to be at the center (nadir) and edge (viewing angle $\approx 45^\circ$, $\phi = 90^\circ$) of the scan. $\tau_a(865)$ was taken to be 0.2, which is about 2-3 times the average for the North Atlantic with a pure maritime atmosphere.²² The results are shown in Figures 3a to 3f (solid lines). There is no value plotted at the scan center for $\theta_0 = 0$ because in that viewing geometry ρ_t would be strongly contaminated by sun glitter. The results suggest that the proposed algorithm is close to producing the ± 0.001 accuracy in the water leaving reflectance at 443 nm under most circumstances.

Figures 3a–3f (dashed lines) also include the error in $t\rho_w$ that the algorithm would have if the correct physics of the atmosphere were single scattering, i.e., if the dotted lines on Figures 2a and 2b were applicable. In this case, $\varepsilon(765, 865)$ is determined exactly, so the error is due entirely to the extrapolation from $\varepsilon(765, 865)$ to $\varepsilon(443, 865)$. Clearly, $t\Delta\rho_w$ is usually larger when there is

significant multiple scattering; however, the results suggest that complications arising from multiple scattering are addressed rather well with the present algorithm.

We have examined other aerosol models that differ considerably from those of Shettle and Fenn,²⁰ e.g., Junge²⁵ power-law distributions with all of the particles characterized by a single, wavelength independent, refractive index. We find that in the case of aerosols for which the size-refractive index distribution is broadly similar to one of the nine candidate models used here, the error is sufficiently small that it can be plotted on the same scale as Figure 3 when $\tau_a(865) = 0.2$. In contrast, when models are used that are not similar to one of our nine basic models, e.g., a model that resembles the Tropospheric aerosol at RH = 70% but with no aerosol absorption, very large errors can occur ($|\Delta\rho| > 0.01$). Thus, it is imperative that the size-refractive index distribution of the N candidate models encompass the actual range of parameters for natural aerosols over the ocean.

To see the influence of the aerosol concentration, we have also carried out simulations with $\tau_a(865) = 0.4$ — a *very* turbid atmosphere over the oceans. Samples of the results for the Maritime aerosol are presented in Figure 4 in which $\Delta\rho$ is compared for $\tau_a(865) = 0.2$ and 0.4. One sees that the algorithm performs nearly as well for the more turbid atmosphere. Figure 4 also includes the results of simulations carried out for a wind-roughened surface.^{13,14} In this case, the wind speed W was 7.5 m/s; however, it was assumed to be zero in the computation of ρ_r , and the algorithm operated as described above. In the cases presented, only a modest gain in accuracy would be achieved by knowing the wind speed.

Finally, we estimate the effect that these errors in the atmospheric correction have on the accuracy of the retrieved pigment concentration. The blue-green radiance ratio given by the semi-analytic model of Gordon et al.²⁶ can be well represented by the expression

$$\log_{10} 3.33C = -1.2 \log_{10} r_L + 0.5(\log_{10} r_L)^2 - 2.8(\log_{10} r_L)^3, \quad (7)$$

where

$$r_L = \frac{1 [L_w(443)]_N}{2 [L_w(550)]_N},$$

and $[L_w(\lambda)]_N$ is the normalized water-leaving radiance¹⁶ at λ , i.e.,

$$tL_w(\lambda) = [L_w(\lambda)]_N \cos \theta_0 \exp \left[- \left(\frac{\tau_r}{2} + \tau_{Oz} \right) \left(\frac{1}{\cos \theta_0} + \frac{1}{\cos \theta} \right) \right].$$

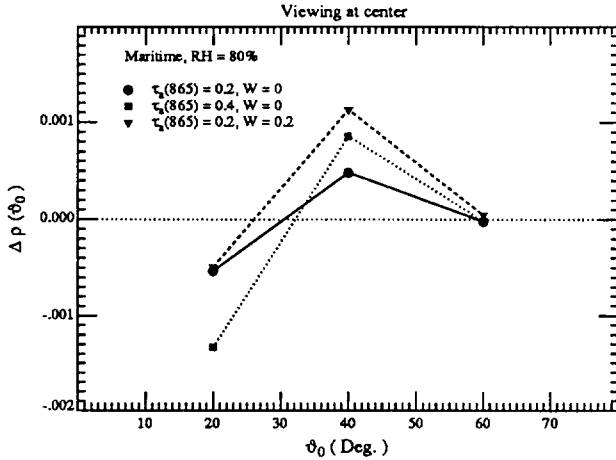


Figure 4a. Examples of the performance of the proposed algorithm at the scan center for a Maritime aerosol when $\tau_a(865)$ is increased from 0.2 to 0.4, or when $\tau_a(865) = 0.2$ but the surface is roughened by a 7.5 m/s wind which is ignored in the operation of the algorithm.

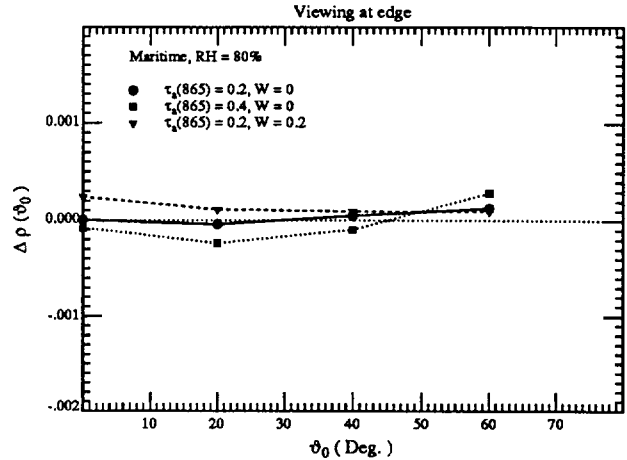


Figure 4b. Examples of the performance of the proposed algorithm at the scan edge for a Maritime aerosol when $\tau_a(865)$ is increased from 0.2 to 0.4, or when $\tau_a(865) = 0.2$ but the surface is roughened by a 7.5 m/s wind which is ignored in the operation of the algorithm.

Approximate values of $[L_w(\lambda)]_N$ for two values of C are given in Table 2. From $\Delta\rho = t\Delta\rho_w$ in

Table 2: $[L_w(\lambda)]_N$ for two pigment concentrations.

C (mg/m ³)	$[L_w(443)]_N$ (mW/cm ² μm Sr)	$[L_w(550)]_N$
0.10	1.65	0.37
0.91	0.34	0.34

Figures 3a-3f, and similar computations at 555 nm, where $t\Delta\rho_w$ is about half of that at 443 nm, it is possible to compute the actual values of $[L_w(\lambda)]_N$ that would be retrieved by the atmospheric correction algorithm. Inserting these into Eq. (7), and neglecting the difference between $\lambda = 550$ nm (used by CZCS) and $\lambda = 555$ nm (to be used in SeaWiFS), the result for the pigment concentration is C' . The error in the retrieved pigment concentration, i.e., $\Delta C = C' - C$, is then determined. It was found that of the 42 simulations $\sim 95\%$ had $\Delta C/C < \pm 30\%$, $\sim 88\%$ had $\Delta C/C < \pm 20\%$, and $\sim 69\%$ had $\Delta C/C < \pm 10\%$. All of the cases with $\Delta C/C > \pm 20\%$ were for $C = 0.91$ mg/m³, where the water-leaving reflectance is very small (~ 0.004) at both wavelengths.

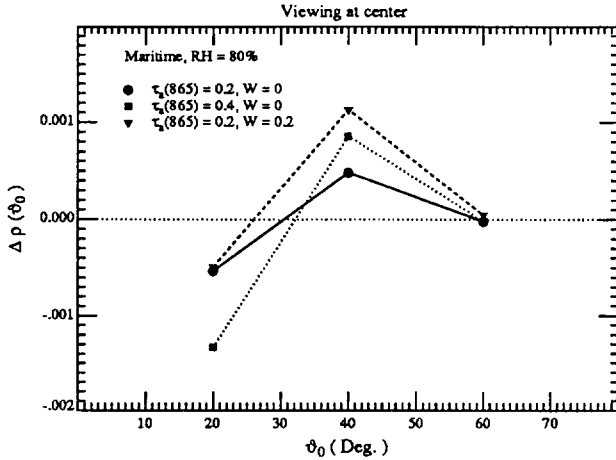


Figure 4a. Examples of the performance of the proposed algorithm at the scan center for a Maritime aerosol when $\tau_a(865)$ is increased from 0.2 to 0.4, or when $\tau_a(865) = 0.2$ but the surface is roughened by a 7.5 m/s wind which is ignored in the operation of the algorithm.

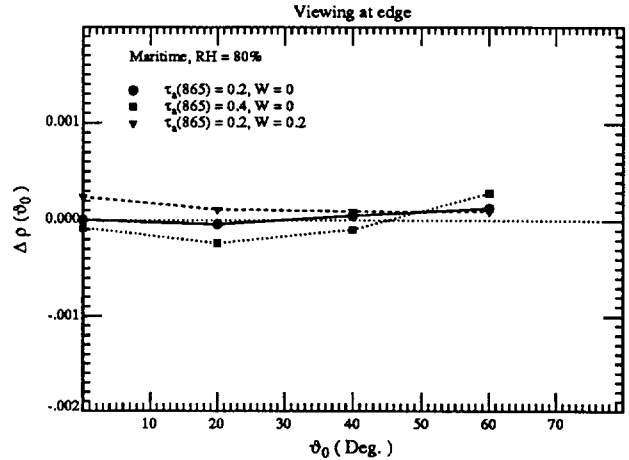


Figure 4b. Examples of the performance of the proposed algorithm at the scan edge for a Maritime aerosol when $\tau_a(865)$ is increased from 0.2 to 0.4, or when $\tau_a(865) = 0.2$ but the surface is roughened by a 7.5 m/s wind which is ignored in the operation of the algorithm.

Approximate values of $[L_w(\lambda)]_N$ for two values of C are given in Table 2. From $\Delta\rho = t\Delta\rho_w$ in

Table 2: $[L_w(\lambda)]_N$ for two pigment concentrations.

C (mg/m ³)	$[L_w(443)]_N$ (mW/cm ² μm Sr)	$[L_w(550)]_N$ (mW/cm ² μm Sr)
0.10	1.65	0.37
0.91	0.34	0.34

Figures 3a-3f, and similar computations at 555 nm, where $t\Delta\rho_w$ is about half of that at 443 nm, it is possible to compute the actual values of $[L_w(\lambda)]_N$ that would be retrieved by the atmospheric correction algorithm. Inserting these into Eq. (7), and neglecting the difference between $\lambda = 550$ nm (used by CZCS) and $\lambda = 555$ nm (to be used in SeaWiFS), the result for the pigment concentration is C' . The error in the retrieved pigment concentration, i.e., $\Delta C = C' - C$, is then determined. It was found that of the 42 simulations $\sim 95\%$ had $\Delta C/C < \pm 30\%$, $\sim 88\%$ had $\Delta C/C < \pm 20\%$, and $\sim 69\%$ had $\Delta C/C < \pm 10\%$. All of the cases with $\Delta C/C > \pm 20\%$ were for $C = 0.91$ mg/m³, where the water-leaving reflectance is very small (~ 0.004) at both wavelengths.

Retrieval of τ_a

There is considerable interest now in the global distribution of aerosols because of their role in climate forcing and biogeochemical cycling.²⁷ The hypothesis²⁸ that dimethylsulfide (DMS) from phytoplankton activity leads to an increase in cloud condensation nuclei in the marine atmosphere argues for simultaneous study of aerosols and productivity where possible.²⁹ There has been effort in recent years directed toward estimating the aerosol concentration ($\propto \tau_a$) and other properties using Earth-orbiting satellites.³⁰⁻³⁹ In this section we show that τ_a can be retrieved with a simple extension of the atmospheric correction algorithm.

Even in the single scattering approximation, one notes from Eq. (4) that it is not possible to estimate τ_a without assuming a model for the aerosol to provide ω_a and P_a . For example, Rao, et al.³⁹ assume that the aerosol consists of spherical particles with a size frequency distribution $\propto (\text{radius})^{-4.5}$ and a refractive index of 1.5. The assumption of an incorrect model can produce significant errors (up to a factor of 2-3) in the recovered τ_a . As in atmospheric correction with SeaWiFS, we will try to avoid using an incorrect model in the retrieval of τ_a by utilizing the only other aerosol information available on a pixel-by-pixel basis — the spectral variation of $\rho_{a\lambda}$.

Our retrieval algorithm is a simple extension of the atmospheric correction algorithm, i.e., the correction algorithm yields the two models which most closely bracket $\varepsilon(765, 865)$, and we use these two models to invert Eq. (4) to obtain two estimates of τ_a . Using the same simulation set we used above to test the correction algorithm, we now examine the accuracy with which τ_a can be estimated. Briefly, we assume that the aerosol consists of particles that are accurately described by the Maritime, Coastal, or Tropospheric aerosol models with RH = 80%. ρ_t is simulated for this aerosol and inserted into the atmospheric correction algorithm. The correction algorithm provides two candidate models based on $\varepsilon(765, 865)$ and these specify two sets of P_a and ω_a values for two estimates of τ_a . These estimates are then averaged to yield the final estimate of τ_a . Tables 3 and 4 provide the % error in the retrieved $\tau_a(865)$ for three aerosol models at the center and the edge of the SeaWiFS scan as a function of θ_0 . The true value of $\tau_a(865)$ was 0.2 or 0.4. All the calculations were carried out for $\phi = 90^\circ$. From the tables, we can see that the error in the retrieved aerosol optical thickness is within $\pm 10\%$ (and usually considerably less) for most of the cases examined.

We also tried determining τ_a from the weighted average of the two estimates as in the correction

Table 3: Error in retrieved $\tau_a(865)$
for viewing at center and edge of the scan. True
value of $\tau_a(865)$ is 0.20.

Position	θ_0	Error (%) in $\tau_a(865)$		
		Maritime	Coastal	Tropospheric
Center	20°	+10.9	-4.74	+2.02
	40°	-2.96	-5.04	+0.62
	60°	-0.31	-4.57	+0.94
Edge	0°	-1.36	-2.69	+0.43
	20°	-1.39	-3.73	+0.13
	40°	-1.75	-5.45	-0.29
	60°	-0.92	-5.74	+0.65

Table 4: Error in retrieved $\tau_a(865)$
for viewing at center and edge of the scan. True
value of $\tau_a(865)$ is 0.40.

Position	θ_0	Error (%) in $\tau_a(865)$		
		Maritime	Coastal	Tropospheric
Center	20°	+9.99	-6.40	+1.01
	40°	-1.82	-6.36	+1.00
	60°	+0.83	-3.63	+1.32
Edge	0°	-0.52	-2.45	+0.99
	20°	-0.24	-2.99	+0.93
	40°	+0.03	-3.77	+0.90
	60°	+0.85	-3.95	+1.37

Table 5: Value of $\tau_a(865)$ required to
saturate SeaWiFS at 865 nm.

Position	θ_0	Maximum value of $\tau_a(865)$	
		Maritime (RH = 98%)	Tropospheric (RH = 70%)
Center	20°	0.72	0.54
	40°	1.04	0.72
	60°	1.69	0.80
Edge	0°	0.88	0.51
	20°	0.98	0.51
	40°	1.04	0.50
	60°	1.02	0.50

algorithm; however, this led to a slightly poorer retrieval.

Finally, it is of interest to estimate the upper limit to the value of $\tau_a(865)$ that can be estimated with SeaWiFS given its design saturation reflectance (ρ_{\max}). This is dependent on the particular aerosol model because for a given τ_a the backscattering (scattering at angles $> 90^\circ$) is strongly dependent on the aerosol size distribution and the refractive index. We estimate the upper limit of $\tau_a(865)$ that can be estimated by using the Tropospheric model with RH = 70% (the *largest* backscattering of the models used here) and the Maritime model with RH = 98% (the *smallest* backscattering). The results are presented in Table 5.

Concluding Remarks

In this paper we have presented an algorithm for atmospheric correction of second generation ocean color scanners with emphasis on SeaWiFS. Two concerns arise in applying the older CZCS algorithm to the more-sensitive SeaWiFS: (1) the extrapolation of the spectral variation of the aerosol reflectance from the NIR into the visible; and (2) the influence of multiple scattering. Realistic aerosol models suggest that the previously-used power law reflectance extrapolation is not likely to be valid (Figure 1) because, although Eq. (6) applies rather well for the CZCS spectral range (443–670 nm), it is sometimes a *very* poor approximation for the SeaWiFS range (412–865 nm). The models also suggest that the effects of multiple scattering depend significantly on the particular aerosol model (Figure 2), i.e., on the aerosol scattering phase function. Thus, it is necessary to have some information regarding the aerosol in order to correctly account for the multiple scattering. Guided by the models we used here, we developed a systematic approach to carrying out the atmospheric correction. The basic hypothesis is that if $\epsilon(765, 865)$ falls between two aerosol models the reflectance $\rho_a + \rho_{ra}$ will fall between the same two models in the same proportion as $\epsilon(765, 865)$. This is certainly not true in general, however, for the range of models we have examined here, it appears to be accurate enough to effect correction to the desired accuracy, even in relatively turbid atmospheres. A simple extension of the algorithm provides an estimate of τ_a with an error of $\pm \lesssim 10\%$.

Our approach to the implementation of these ideas is to create a set of look up tables in which $\rho_t - \rho_r - t\rho_w$ is provided as a function of ρ_{as} (Figure 2). These tables will consist of several aerosol models which must encompass the expected natural range of the size-refractive index distribution), aerosol optical thicknesses, and all possible combinations of solar and viewing

geometries. Operation of the algorithm will be similar to that presented above, with the adaptation to the particular geometry made by interpolation. Since application of this new algorithm requires derivation of an accurate value for $\epsilon(765, 865)$, high radiometric calibration is a necessity, as well as removal of any component of ρ_t that is due to whitecaps^{40,41} on the sea surface. Also, the 765 nm band overlaps the O₂ absorption band at 759 nm, so its influence on $\rho_t(765)$ needs to be assessed. We view all three of these requirements as major challenges; however, the O₂ absorption problem can be circumvented by utilizing the 670 nm band in place of the 765 nm band at the expense of having to assess $\rho_w(670)$ in waters with $C \gtrsim 1 \text{ mg/m}^3$.

We are not really comfortable with an atmospheric correction algorithm that makes such extensive use of aerosol models. The difficulty with the models is twofold. First, although they were developed on the basis of measurements of the size distribution and index of refraction of aerosol particles, they are obvious simplifications of the actual physical-chemical properties of the aerosol. Second, their optical properties have been computed using Mie theory, i.e., assuming homogeneous spherical particles. Such a simplification may yield realistic scattering and extinction coefficients, but could result in significant errors in the computed phase function,⁴² particularly in the important backscattering directions. Our hope is that they provide a realistic approximation for $\epsilon(\lambda_i, \lambda_j)$ and the multiple scattering effects. However, at this point we see no more rational approach for achieving the required accuracy, considering that the effects of multiple scattering are model dependent. In the final analysis, their efficacy must be judged on the quality of the atmospheric correction that they produce.

Finally, we should remark that the proposed correction algorithm could also be based on measured, column-averaged, optical properties of the aerosol, e.g., obtained by inverting at-sea sky radiance and sun photometer measurements⁴³ to obtain $\tau_a(\lambda)$, $\omega_a(\lambda)$, and $P_a(\alpha, \lambda)$ — the optical properties that the models provide. A comprehensive data base of such properties would circumvent the reliance on aerosol models and place the correction algorithm on a firmer foundation.

References

- [1] W. A. Hovis, D. K. Clark, F. Anderson, R. W. Austin, W. H. Wilson, E. T. Baker, D. Ball, H. R. Gordon, J. L. Mueller, S. Y. E. Sayed, B. Strum, R. C. Wrigley and C. S. Yentsch, "Nimbus 7 coastal zone color scanner: system description and initial imagery," *Science* **210**, 60–63 (1980).
- [2] H. R. Gordon, D. K. Clark, J. L. Mueller and W. A. Hovis, "Phytoplankton pigments derived from the Nimbus-7 CZCS: initial comparisons with surface measurements," *Science* **210**, 63–66 (1980).
- [3] H. R. Gordon and A. Y. Morel, *Remote Assessment of Ocean Color for Interpretation of Satellite Visible Imagery: A Review* (Springer-Verlag, New York, 1983), 114 pp.
- [4] S. B. Hooker, W. E. Esaias, G. C. Feldman, W. W. Gregg and C. R. McClain, *SeaWiFS Technical Report Series: Volume 1, An Overview of SeaWiFS and Ocean Color* (NASA Technical Memorandum 104566, July 1992).
- [5] V. V. Salomonson, W. L. Barnes, P. W. Maymon, H. E. Montgomery and H. Ostrow, "MODIS: Advanced Facility Instrument for Studies of the Earth as a System," *IEEE Geosci. Rem. Sens.* **27**, 145–152 (1989).
- [6] H. R. Gordon, "Radiative Transfer: A Technique for Simulating the Ocean in Satellite Remote Sensing Calculations," *Applied Optics* **15**, 1974–1979 (1976).
- [7] H. R. Gordon, "Removal of Atmospheric Effects from Satellite Imagery of the Oceans," *Applied Optics* **17**, 1631–1636 (1978).
- [8] H. R. Gordon and D. K. Clark, "Atmospheric effects in the remote sensing of phytoplankton pigments," *Boundary-Layer Meteorology* **18**, 299–313 (1980).

- [9] H. R. Gordon, D. K. Clark, J. W. Brown, O. B. Brown, R. H. Evans and W. W. Broenkow, "Phytoplankton pigment concentrations in the Middle Atlantic Bight: comparison between ship determinations and Coastal Zone Color Scanner estimates," *Applied Optics* **22**, 20–36 (1983).
- [10] M. Viollier, D. Tanre and P. Y. Deschamps, "An algorithm for remote sensing of water color from space," *Boundary Layer Meteorology* **18**, 247–267 (1980).
- [11] H. R. Gordon and D. J. Castaño, "The Coastal Zone Color Scanner Atmospheric Correction Algorithm: Multiple Scattering Effects," *Applied Optics* **26**, 2111–2122 (1987).
- [12] H. R. Gordon, J. W. Brown and R. H. Evans, "Exact Rayleigh Scattering Calculations for use with the Nimbus-7 Coastal Zone Color Scanner," *Applied Optics* **27**, 862–871 (1988).
- [13] H. R. Gordon and M. Wang, "Surface Roughness Considerations for Atmospheric Correction of Ocean Color Sensors. 1: The Rayleigh Scattering Component," *Applied Optics* **31**, 4247–4260 (1992).
- [14] H. R. Gordon and M. Wang, "Surface Roughness Considerations for Atmospheric Correction of Ocean Color Sensors. 2: Error in the Retrieved Water-leaving Radiance," *Applied Optics* **31**, 4261–4267 (1992).
- [15] P. Y. Deschamps, M. Herman and D. Tanre, "Modeling of the atmospheric effects and its application to the remote sensing of ocean color," *Applied Optics* **22**, 3751–3758 (1983).
- [16] H. R. Gordon and D. K. Clark, "Clear water radiances for atmospheric correction of coastal zone color scanner imagery," *Applied Optics* **20**, 4175–4180 (1981).
- [17] A. Bricaud and A. Morel, "Atmospheric Corrections and Interpretation of Marine Radiances in CZCS Imagery: Use of a Reflectance Model," *Oceanologica Acta* **7**, 33–50 (1987).

- [18] J. -M. André and A. Morel, "Atmospheric Corrections and Interpretation of Marine Radiances in CZCS Imagery, Revisited," *Oceanologica Acta* **14**, 3-22 (1991).
- [19] G. C. Feldman, N. Kuring, C. Ng, W. Esaias, C. R. McClain, J. Elrod, N. Maynard, D. Endres, R. Evans, J. Brown, S. Walsh, M. Carle and G. Podesta, "Ocean Color: Availability of the Global Data Set," *EOS Trans. Amer. Geophys. Union* **70**, 634-641 (1989).
- [20] E. P. Shettle and R. W. Fenn, *Models for the Aerosols of the Lower Atmosphere and the Effects of Humidity Variations on Their Optical Properties* (Air Force Geophysics Laboratory, Hanscomb AFB, MA 01731, AFGL-TR-79-0214, 1979).
- [21] F. X. Kenizys, E. P. Shettle, W. O. Gallery, J.H.Chetwynd, L. W. Abreu, J. E. A. Selby, S. A. Clough and R. W. Fenn, *Atmospheric Transmittance/Radiance: The LOWTRAN 6 Model* (Air Force Geophysics Laboratory, Hanscomb AFB, MA 01731, AFGL-TR-83-0187, 1983) NTIS AD A137796.
- [22] P. J. Reddy, F. W. Kreiner, J. J. Deluisi and Y. Kim, "Aerosol Optical Depths Over the Atlantic Derived From Shipboard Sunphotometer Observations During the 1988 Global Change Expedition," *Global Biogeochemical Cycles* **4**, 225-240 (1990).
- [23] M. Wang and H. R. Gordon, *Remote Sensing of Environment* (1993), "A Simple, Moderately Accurate, Atmospheric Correction Algorithm for SeaWiFS" (Submitted).
- [24] M. Wang, "Atmospheric Correction of the Second Generation Ocean Color Sensors," 1991, Ph.D. Dissertation, University of Miami, Coral Gables FL, 135 pp.
- [25] C. Junge, "Atmospheric Chemistry," *Advances in Geophysics* **4**, 1-108 (1958).
- [26] H. R. Gordon, O. B. Brown, R. H. Evans, J. W. Brown, R. C. Smith, K. S. Baker and D. K. Clark, "A Semi-Analytic Radiance Model of Ocean Color," *Jour. Geophys. Res.* **93D**, 10909-10924 (1988).